Separation of chiral nanotubes with an opposite handedness by chiral oligopeptide adsorption: A molecular dynamics study

Giuseppina Raffaini*, Fabio Ganazzoli

Dipartimento di Chimica, Materiali e Ingegneria Chimica 'G. Natta', Politecnico di Milano, and Unità Politecnico INSTM, Piazza Leonardo da Vinci 32, 20133 Milano, Italy

Received 29 September 2015
Received in revised form 2 November 2015
Accepted 10 November 2015
Available online 25 November 2015

1. Introduction

Carbon nanotubes, including multi-walled and in particular single-walled carbon nanotubes (SWNT), have spurred a large interest in the last years for their most peculiar structure, leading to new and unusual electronic and structural properties, relevant for nanoscience in general, but in particular for electronic, mechanical and biomaterials applications [1–4]. SWNT can be structurally described as the cylindrical wrapping of a single graphene sheet, and are structurally characterized with two indices, (n, m): in particular, if $n = m$ one gets the so-called armchair nanotubes, which are electrically conducting, whereas for $n \neq m$ one gets the chiral nanotubes, where the nanotube chirality is akin to the chirality of the isotactic stereoregular polymers having a helical conformation in the solid state. The latter SWNTs (which are in most cases semiconducting, apart from special combinations of the n, m indices) are often denoted as nanotubes with different chiralities with reference to the chiral vector characterized by the (n, m) values which describe how the graphene sheet is wrapped up [5]. In a more rigorous chemical language, however, a different chirality indicates molecules that are non-superimposable to their mirror images, so that it refers to individual enantiomeric (n, m) and (m, n) nanotubes [6], which accordingly differently respond to circularly polarized light. Incidentally, we also mention that enantiomeric nanotubes are sometimes denoted as M and P nanotubes with a single set of values (n, m) and $n > m$ [7].

Because of this feature, enantiomeric SWNTs may in principle interact with chiral molecules by forming complexes with an unlike stability, thus allowing separation of left-handed from right-handed nanotubes for instance through appropriate chromatographic procedures with suitable stationary phases. Such separation of enantiomeric carbon nanotubes was first achieved experimentally by using chiral nano-tweezers formed by two porphyrin rings joined by a 1,3-substituted phenyl ring, each carrying two asymmetric substituents [7,8]. Another successful separation technique employed density gradient ultracentrifugation using a chiral sodium cholate surfactant [9]. The chiral recognition of nanostructured carbon allotropes (nanotubes or fullerenes) is thus an emerging area of great potential interest [10], related also to their effect in the formation of chiral molecules in certain chemical reactions [11]. On the other hand, such experimental achievements were quite unexpected on the basis of earlier theoretical results for the adsorption of *trans* 1,2-substituted cyclopropane and cyclohexane on chiral SWNT [12]. In the latter work, a united atom model

* Corresponding author. Tel.: +39 0223993068; fax: +39 0223993180.
E-mail address: giuseppina.raffaini@polimi.it (G. Raffaini).

Table 1
The sequence of residues in the selected amino acid sequence with the corresponding hydropathy indices.

Residue	Hydropathy index[a]
GLU16	−3.5
GLU17	−3.5
ASN18	−3.5
PHE19	2.8
LYS20	−3.9
ALA21	1.8
LEU22	3.8
VAL23	4.2
LEU24	3.8
ILE25	4.5
ALA26	1.8
PHE27	2.8
ALA28	1.8
GLN29	−3.5
TYR30	−1.3
LEU31	3.8

[a] [29].

was adopted for the adsorbates interacting with the SWNT through a Lennard-Jones potential. Using a hybrid Monte Carlo method at a constant temperature and considering chiral SWNT of different diameters, the difference in stability of the chiral adsorbates inside the enantiomeric nanotubes was always found to be smaller than about 65 J/mol, but with an even larger statistical uncertainty which indicated than no enantioselectivity should actually be possible. Since this result is clearly at variance with the abovementioned experimental results, we can speculate that the number of asymmetric chiral atoms present in the experimentally used adsorbate molecules and their flexibility can explain this discrepancy, and furthermore that using a fully atomistic theoretical model could also be most relevant.

Therefore, in order to tackle this issue, we decided to consider an oligopeptide formed by natural amino acids that contain multiple chiral centers and form a α-helix in the native state, and to model its adsorption on enantiomeric SWNTs with fully atomistic molecular mechanics (MM) and molecular dynamics (MD) methods. We recently modeled the adsorption of larger protein subdomains comprising 60 amino acids mostly structured in three α-helices on achiral, armchair SWNT, more precisely the (30, 30), (40, 40) and (50, 50) nanotubes, considering both the outer convex and the inner concave surface to understand the effect of an unlike nanoscale topography (the different radii of curvature), and the adsorption a single oligopeptide within the much smaller (8, 8) and (10, 10) SWNT [13]. Conversely, the aim of the present study is to determine whether a chiral oligopeptide formed by natural amino acids can discriminate between two chiral enantiomeric SWNTs, namely the (10, 20) and (20, 10) nanotubes, of opposite handedness by forming non-covalent complexes with an unlike stability. Adopting throughout the same methodology as in our previous work [13], in this study the chosen oligopeptide is a hydrophobic sequence with a native α-helix structure taken from human serum albumin (HSA), more precisely helix A2A formed by 16 residues, from GLU16 to LEU31 as reported in Table 1, previously employed also to model the interaction with the (8, 8) and (10, 10) SWNT [13]. This α-helix belongs to a subdomain close to the outer HSA envelope (see Fig. 1 of ref. [14]), but still it is quite hydrophobic, as shown by the hydropathy indices of the individual residues reported in Table 1.

It should be added that all residues in the chosen sequence contain a chiral C_α atom, since glycine is not present. The selected nanotubes are two uncapped chiral SWNT (n, $2n$) and ($2n$, n), with $n = 10$, having a diameter of 20.71 Å, but for comparison we also modeled adsorption on an achiral armchair (16, 16) SWNT with a diameter of 21.70 Å. In all cases, we considered the oligopeptide interaction with the inner concave and with the outer convex nanotube surfaces, thus having two unlike topographies but the same surface chemistry of sp^2 carbon atoms. In either case, however, we assumed an unbiased interaction by placing the starting oligopeptide helix with different initial arrangements close to the lateral surface and to the open end of the nanotubes, not assuming any a priori insertion within the SWNT. Thus, surface adsorption or encapsulation of the oligopeptide would only take place within the MD runs if indeed the surface interaction is favorable.

In the following, after a short description of the simulation methodology, we discuss the oligopeptide interaction strength with the outer or the inner nanotube surfaces and the general stability of the resulting adducts after its adsorption and spreading with complete denaturation. Afterwards, we describe in more detail the interaction geometries, first inside the SWNT on the concave surface, and then outside the SWNT on the convex surface, considering the system energy and the adsorbate conformation through the Ramachandran maps. Further details about the simulations results can be found in the Supplementary data. The present simulations are carried out in an effective dielectric medium using a distance-dependent dielectric constant as done in previous papers [13–17]. This approach allows probing lengthy large-scale surface rearrangements thanks both to the smaller system size and to the much faster relaxation rate due to the lack of friction with the solvent molecules. Such approach was already supported by a comparison with our previous simulations in explicit water, where the changes in the solvation energy was estimated to amount to about 10% [17], and with our simulations of molecular recognition phenomena in supramolecular host–guest complexes [18]. Moreover, using MD simulations in explicit water [19,20], Szeifler et al. [19] recently showed that atomistic MD simulations of protein adsorption (lysozyme) on a hydrophobic surface (namely crystalline polyethylene) require huge simulation times because of lengthy dehydration processes, but eventually, after an initial diffusion to the surface, the protein–surface interaction leads to their dehydration on timescales of the order of tens of nanoseconds, eventually followed by local denaturation mostly involving the loss of α-helices. Moreover, Zhou et al. [20] showed that a much smaller protein (the villin headpiece, comprising only 35 residues) on graphene in explicit water lead to a very large, though not yet fully complete, surface spreading. Such adsorption processes, accompanied by very lengthy protein dehydration close to the surface, produced final arrangements very similar to those obtained by us on graphite with the effective dielectric medium, thus supporting our use of an implicit solvent as a way to significantly speed up computationally the protein adsorption process on these materials without introducing significant artifacts.

2. Simulation method

The simulations were performed using the same methodology adopted in our previous papers, using the InsightII/Discover, the Materials Studio and the Discovery Studio programs [21] with the consistent valence force field CVFF [22], as previously done in similar studies [13–17]. We considered uncapped chiral (10, 20) and (20, 10) SWNTs with a diameter $D = 20.71$ Å and a length of 67.63 Å, and an armchair (16, 16) SWNT with $D = 21.70$ Å and a length of 61.49 Å. The selected oligopeptide sequence was taken as the hydrophobic A2A α-helix of human serum albumin (described in more detail in ref. [14] and previously modeled also in ref. [13]) containing 16 residues (all with a chiral C_α atom, since glycine is not present) with the appropriate charges for the ionizable residues at the physiological pH = 7.4. The native α-helix was optimized close to the surfaces in four unbiased trial orientations both close to one open end of the uncapped SWNTs, not assuming a priori any inclusion

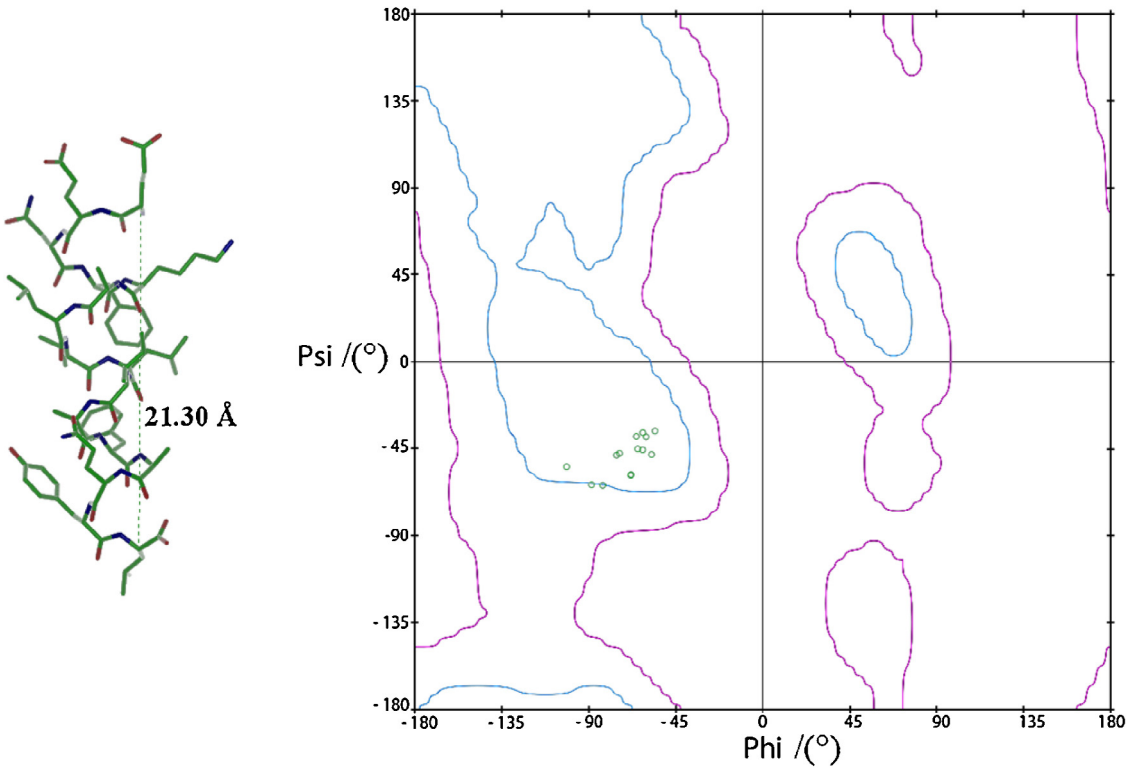

Fig. 1. The native α-helix structure of the selected oligopeptide is shown at left (bonds to the O atoms are shown in red and to N atoms in blue, while H atoms were omitted for clarity), its length being shown by the green dotted line joining the first and the last C_α atom, while the Ramachandran map at right shows the Ψ and Φ values of the torsion angles adjacent to the C_α atoms. The blue and red lines in the Ramachandran map respectively highlight the basins of the most probable and of the observed range of values observed in current proteins. (For interpretation of the references to color in this figure legend, the reader is referred to the web version of this article.)

geometry, and near the outer surface so as to mimic a random approach from the solution. The energy minimizations were carried out up to an energy gradient lower than 4×10^{-3} kJ mol^{-1} Å^{-1} in an implicit solvent using a distance-dependent dielectric constant [13–17], keeping fixed the carbon atoms of the nanotubes. The MD runs were performed in the same implicit solvent at a constant temperature (T = 300 K) controlled through the Berendsen thermostat. Integration of the dynamical equations was carried out with the Verlet algorithm using a time step of 1 fs, and the instantaneous coordinates were periodically saved for further analysis or geometry optimization. Within the MD runs, we monitored the time changes of the total and potential energy together with its components, and the distance between the protein center of mass and the surface. In general, these quantities showed a fast initial decrease, and then fluctuated around a constant value, indicating achievement of equilibrium, which always required much less than the 2 ns of the adopted simulation time. The final optimizations were carried out with the same convergence criteria as before.

3. Results and discussion

The selected oligopeptide contains 16 residues, all with a chiral C_α atom, and is mainly hydrophobic, a few polar residues being present near the two ends, as shown in Table 1. The length of the native α-helix reported in Fig. 1, defined as the distance between the C_α atoms of the first and the last residue, amounts to 21.30 Å, almost equal to the diameters of the SWNTs considered here. The secondary helical structure of the native oligopeptide is also evidenced by the typical Ψ and Φ values of the torsion angles adjacent to the C_α carbons, as shown by the Ramachandran map in Fig. 1: thus, the Φ and the Ψ values are distributed in the range between −45° and −110° and between −30° and −60°, respectively.

3.1. Adsorption stability on the (10,20), (20,10) and (16,16) SWNT

As already pointed out, unlike what done in our previous work, where we considered protein adsorption and achiral SWNT [13], we selected two enantiomeric chiral nanotubes, namely, the (10, 20) and (20, 10) SWNT having a diameter of 20.71 Å, and furthermore a similar-sized achiral armchair (16, 16) SWNT with a diameter of 21.70 Å for a comparison. The choice of these three nanotubes was obviously due to their diameter, closely matching the helical length. As initial trial geometries of the oligopeptide close to each nanotube, we considered in all cases an outer position with four arrangements of the oligopeptide close to an open end and four arrangements close to the lateral surface of the nanotubes, see for instance Fig. S1 of the Supplementary data. Both close to the open end and close to the lateral nanotube surface, two starting arrangements had the helical axis parallel or perpendicular to the nanotube axis, considering two possible arrangements rotated by 180° around an axis orthogonal to the helical axis. In view of the nanotube shape, in each case one orientation is in principle redundant, but it was kept to check for the robustness of the results and to enhance their reliability. We first optimized all the abovementioned trial geometries of the oligopeptide near the outer surface and near the open end of the three SWNT (see for instance Fig. S2), and calculated for each optimized geometries the potential energy and the interaction energy of these initial adsorption stages. Using the simulation protocol described in Section 2 (see also refs. [13–17]), and starting from both the most and the least stable geometries just obtained, we followed the time evolution of the system at room temperature through the MD runs. In this way, we searched for the most stable states achieved by the oligopeptide near the outer surface and close to the open end, or better inside the SWNT (see also later), considering four geometries (the most and the least stable in the initial stage, on the outer and on the inner

Table 2
The interaction energy E_{int}, the strain energy E_{strain} and the potential energy E_{pot} (kJ/mol) for the oligopeptide adsorption on the inner and the outer surfaces of the different SWNTs. The starred values are the values normalized by the number of the 16 residues of the oligopeptide. For each surface, the first two lines apply to the most stable state, and the other two to the metastable state.

Chiral (20, 10) SWNT			Chiral (10, 20) SWNT			Armchair (16, 16) SWNT		
E_{int}	E_{strain}	E_{pot}	E_{int}	E_{strain}	E_{pot}	E_{int}	E_{strain}	E_{pot}
Inner surface								
−1397	111	572(1) ± 23	−1320	181	654(1) ± 25	−1338	186	634(1) ± 24
−87.3*	6.92*		−82.5*	11.3*		−83.6*	11.6*	
−1353	189	621(1) ± 23	−1165	68	806(1) ± 25	−1290	188	684(1) ± 23
−84.6*	11.84*		−83.2*	4.8*		−80.6*	11.8*	
Outer surface								
−787	151	1191(1) ± 24	−735	109	1242(1) ± 27	−789	170	1188(1) ± 25
−49.2*	9.4*		−45.9*	6.8*		−49.3*	10.6*	
−749	179	1237(1) ± 27	−686	190	1297(1) ± 24	−776	219	1204(1) ± 27
−46.8*	11.2*		−42.8*	11.9*		−48.5*	13.7*	

surface) for each nanotube. Finally, we determined the optimized geometries assumed after the system equilibration by minimizing twenty conformations saved during the last part of the MD run.

The interaction of the oligopeptide with the two enantiomeric chiral SWNT, either on the inner or on the outer surface, may produce two different non-covalent adducts, as mentioned before: according to the present simulations, such adducts displayed a significantly unlike stability. This stability can be measured through the interaction energy E_{int} calculated for the most stable state after optimizing many instantaneous snapshots periodically saved along the dynamic trajectory, and through the average potential energy E_{pot} obtained within the MD run at 300 K reported in Table 2. The interaction energy is defined as $E_{int} = E_{tot} - (E_{free} + E_{substr})$, where E_{tot} is the energy of the whole system, E_{free} is the energy of the free native oligopeptide, and E_{substr} is the energy of the nanotube substrate (in the present case it is a constant conveniently set to zero since the SWNT is kept fixed). We incidentally note here that we previously defined E_{int} with the opposite sign [13], so that $E_{int} > 0$ would correspond to the energy required to desorb the protein fragment from the surface and bring it back to the free native state, unlike the present definition. On the other hand, in the present case a lower E_{int} implies a stronger adsorption, just as a lower E_{pot} does, monitored, however, within the dynamic run at room temperature. In turn, the potential energy (with respect to an arbitrary zero) can be obtained by the average value calculated after equilibration in the last 1 ns of the MD trajectory at 300 K. These values are also reported in Table 2 together with their standard error in parentheses and their standard deviations.

In Table 2, we also report the strain energy, E_{strain}, corresponding to the energy penalty undergone by the oligopeptide upon adsorption compared to the native geometry. Accordingly, it is defined as $E_{strain} = E_{frozen} - E_{free}$, where E_{frozen} is the oligopeptide energy in the frozen geometry it adopts upon adsorption [13–17]. For each SWNT and each surface (i.e., the inner and the outer one), Table 2 contains these energy values both for the most stable state and for the first metastable state with a higher energy: according to the current practice, we define as most stable state and first metastable state the states with the lowest and the next-to-lowest local energy minima obtained by optimization of many (20) instantaneous snapshots saved in the MD runs, or with the lowest and the next-to-lowest average potential energy obtained in the MD runs at 300 K. For a comparison with previous results [13] (where an unlike choice of sign was adopted, as just mentioned), Table 2 reports also the intrinsic values of E_{int} and E_{strain} through the starred values normalized by the number of amino acids in contact with the surface, $n_{5\,Å}$, where 5 Å is conveniently taken as the upper distance for a contact interaction, as done before [13–17]. Note that, in general, all the 16 residues were in contact with the surface, apart from a single metastable state. It should also be noted that the stability order and the energy differences are the same both considering the interaction energy calculated with the minimized energies (i.e., at 0 K) and the potential energy obtained within the MD run for systems subject to the thermal fluctuations at room temperature (300 K).

As anticipated, the two non-covalent adducts formed by the chiral oligopeptide with the two enantiomeric SWNT show a markedly different stability. In particular, Table 2 shows that the most stable final state is achieved on the (20, 10) SWNT either considering the inner concave surface or the outer convex surface. This larger stability is displayed both through a lower (i.e., more negative) E_{int}, indicating a stronger adsorption, and through a smaller E_{pot} in the MD run at room temperature on the (20, 10) SWNT than on the (10, 20) SWNT. Interestingly, we also find a larger stability on the former nanotube not only through the most stable state, but even in terms of the first metastable state of the (20, 10) SWNT that is even more stable than the best arrangement on the (10, 20) SWNT with a lower E_{int} and a smaller E_{pot}. We further stress that such result applies both for the outer and for the inner surface. It is also of interest to note that the interaction strength of the oligopeptide with the non-chiral armchair (16, 16) SWNT is somehow intermediate between the two extremes of the chiral nanotubes when adsorption takes place on the inner surface, being however quite closer to the interaction strength of the (10, 20) SWNT. On the other hand, if we consider the outer surface, the adsorption strength on the armchair nanotube is as large as in the case of the chiral (20, 10) SWNT, and accordingly it is larger than on the (10, 20) SWNT. We can visually summarize this discussion about the complex stability by the picture shown in the following Fig. 2, which points out that the separation of chiral nanotubes of opposite handedness is indeed feasible.

Let us now briefly describe the adsorption geometry and the surface arrangement of the adsorbed oligopeptide on the inner and on the outer SWNT surface.

3.2. *Interaction on the inner surface of the SWNT*

When the oligopeptide was placed close to the open end of a nanotube in its native α-helical structure (Fig. S1*a*), the preliminary energy optimization produced in any case a favorable interaction often leading to encapsulation of the oligopeptide inside the SWNT (see Fig. S2). This process took place upon the initial optimization in all cases for the armchair (16, 16) SWNT, while it was obtained in three out of four cases for the chiral SWNTs: in fact, insertion was always found when the helical axis was parallel to the SWNT axis, whereas when it was perpendicular but pointing in opposite directions, we found for each chiral SWNT either insertion or an outer interaction at the nanotube open rim. Moreover, inside the (16, 16) SWNT, the helical conformation of the oligopeptide was loosely preserved if the helical axis was initially parallel to the nanotube axis, the main deformations involving the terminal residues,

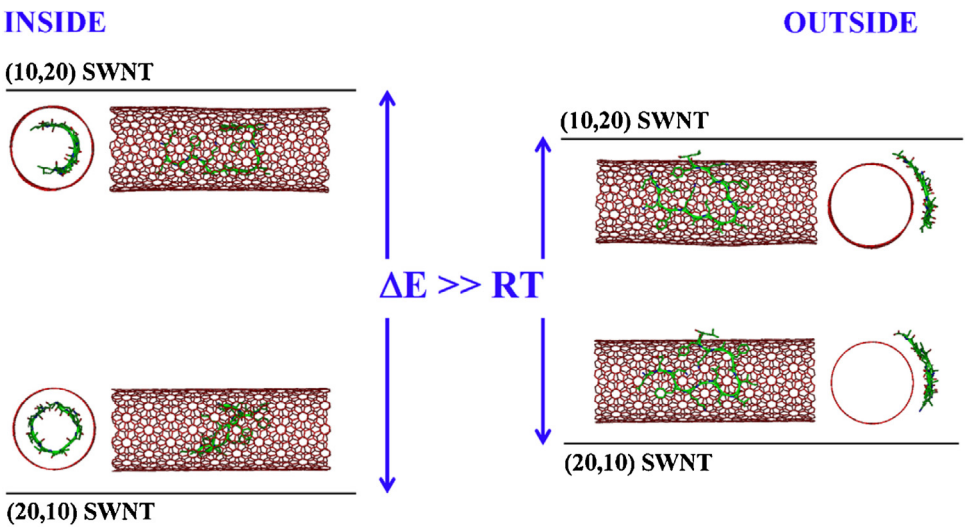

Fig. 2. The larger stability of the complex formed by the oligopeptide adsorbed either on the inner or on the outer surface of the (20, 10) SWNT is pictorially shown.

whereas larger deformations were found in a perpendicular position. Similar results were arrived at with the chiral nanotubes, but in this case when the helical axis was placed perpendicular to the nanotube axis we found insertion only in one case out of two, again with relatively minor distortions. On the other hand, a true helical structure (even though a shortened one) is generally preserved after these initial optimizations inside the (20, 10) SWNT, whereas only loose helicoidal features or full denaturation are found inside the (10, 20) SWNT. In all cases, the most and the least stable geometry obtained by these initial optimizations were used as starting geometries for the independent MD runs, until equilibration was achieved, as monitored for instance through the time changes of the potential energy and its components (see for instance Figs. S3*a*–S5*a*) and of the distance between the centers of mass of the oligopeptide and the nanotube. Finally, we performed the energy minimizations of many instantaneous snapshots to find the best adsorption geometries.

The most stable final state was eventually achieved inside the (20, 10) SWNT, where the denatured oligopeptide assumes a relatively elongated conformation fully wrapping the inner surface and almost forming a ring roughly perpendicular to the nanotube axis (see Fig. 3), similar to what was previously found on armchair SWNTs [13]. In this way, all the residues are in contact with the surface, together with their (largely hydrophobic) side groups: in particular the aromatic rings of the two PHE and of the TYR amino acids showing intermolecular π–π interactions, and the alkyl chains of the two LEU and of the ILE amino acids with intermolecular C—H–π interactions. Moreover, the system stability is also enhanced by two intramolecular hydrogen bonds involving the side groups of two second neighboring residues. These results for the main interactions between the amino acids and the surface and among themselves are in agreement with our earlier results on armchair nanotubes [13]. They are also similar to those found in a molecular dynamics study of an oligopeptide adsorbed in water on graphene and on a (0, 15) SWNT [23]. Accordingly, the interaction energy is smallest, and the intrinsic E_{int} (i.e., the interaction energy divided by the number of residues in contact with the surface) amount to −87.3 kJ/mol, as shown in Table 2. Interestingly, this value is significantly lower than the value found on the inner surfaces of larger SWNT, following the same general trend already pointed out by us [13]: on a concave surface the intrinsic E_{int} becomes lower (according to the present choice of sign) with a decreasing radius or curvature, or with a decreasing diameter. It is also important here to stress that the second best geometry is again achieved in a metastable state on the inner surface of the same (20, 10) SWNT, also reported in Table 2: in this case, the interaction is weaker than in the most stable state by more than 40 kJ/mol, and correspondingly the intrinsic E_{int} is also somewhat larger. This weaker interaction is partly due to a less favorable interaction with the surface, but also largely due to a higher penalty imposed (embodied in E_{strain}) to the deformed oligopeptide strongly elongated in the direction of the nanotube axis, leading to the formation of one intramolecular H bond only (Fig. 3).

The surface interaction is weaker on the enantiomeric (10, 20) SWNT: in the most stable arrangement, the oligopeptide is quite, but not fully, elongated in the direction of the nanotube axis, but it does not form any intramolecular H bond. The surface arrangements of the side chains are apparently very similar to those achieved on the enantiomeric SWNT, but require somewhat larger deformations, hence a larger strain energy and a slightly smaller intrinsic E_{int}. On the other hand, in the metastable state found inside the (10, 20) SWNT, some significant difference is found (Fig. 3 at right). Here, in fact, not all residues interact with the surface, since two of them remain near the nanotube central axis: in particular, the phenol group of TYR, topologically close to one end, is clearly visible in the figure. In this way, the first and the last amino acid of the zwitterionic oligopeptide can strongly interact through electrostatic interactions and hydrogen bonds. However, since some favorable dispersive interactions with the surface are lost, involving in particular an aromatic ring, the overall stability of this geometry is less than in the other cases, and the intrinsic E_{int} is a bit larger (i.e., less negative) than in the other cases (see Table 2).

It is also of interest to mention that the somewhat different final geometries achieved inside the two enantiomeric SWNTs (Fig. 3 at left) are also reflected in some difference in the dynamic trajectories. In fact, within the MD run, we found a rather general pattern, whereby the oligopeptide underwent first a fast shuttling motion parallel to the nanotube axis, and then at equilibrium a slower one both on the inner surface, and parallel to the nanotube axis with a smaller excursion (see the .AVI files in the Supplementary data). Initially, this motion can be followed through the distance between the center of mass (c.o.m.) of the oligopeptide and the c.o.m. of the nanotube as shown in Fig. 4 for the most stable state eventually achieved inside the (20, 10) and the (10, 20) SWNT.

It can be noted that at equilibrium in the former case the positions of the c.o.m. of the oligopeptide fluctuate around a position that coincides with the c.o.m. of the nanotube, while this is not so in the latter case because of the different geometry maintained on

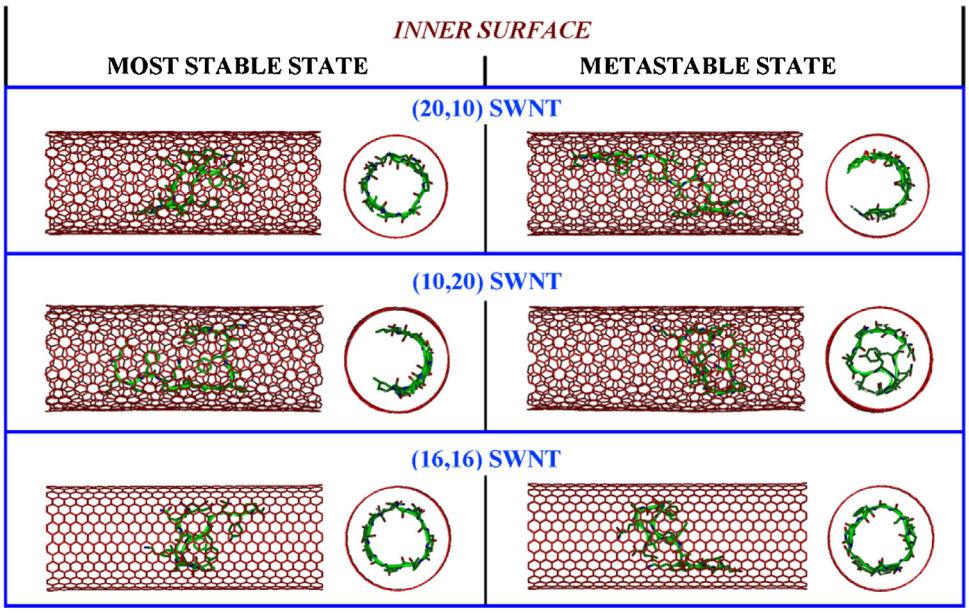

Fig. 3. The most stable (left column) and the metastable state (right column) eventually achieved by the oligopeptide inside the (20, 10), the (10, 20) and the (16, 16) SWNT (top to bottom) viewed side on and end on in each case.

the concave surface: as clearly seen in the end-on view in Fig. 3, the two c.o.m. may well coincide within the MD trajectory for the (20, 10) SWNT, unlike what seen in the enantiomeric nanotube because of the different arrangement (the oligopeptide c.o.m. is outside the nanotube axis).

To put in perspective the results about the unlike stability of the oligopeptide adsorbed on the enantiomeric SWNTs, we also report the analogous results on the armchair (16, 16) SWNT, which basically has the same diameter as the two chiral nanotubes. In the most stable state inside this nanotube, the oligopeptide assumes roughly the same arrangement as in the most stable of all states, which was achieved inside the (20, 10) SWNT (see Fig. 3), being only slightly more elongated along the nanotube axis. Moreover, the side groups do also interact favorably with the surface in a way quite similar to that described on the latter nanotube. However, the unlike non-chiral nature of the carbon surface in this armchair nanotube makes this arrangement less favorable than inside the (20, 10) SWNT, due also to a larger strain energy. On the other hand, insertion within the (16, 16) SWNT is found to be more stable than inside the (10, 20) SWNT, as clearly seen from Table 2. Correspondingly, the intrinsic E_{int} obtained for the armchair nanotube is also intermediate between those found for the two enantiomeric chiral SWNT, even though it qualitatively follows the general trend obtained with other armchair nanotubes [13]. Inside the armchair (16, 16) SWNT, in the most stable state all the residues optimally interact with the surface, in particular through the aromatic rings (phenyl rings of two PHE and phenol ring of one TYR) parallel to the surface with intermolecular π–π interactions. Moreover, the oligopeptide also optimizes the intramolecular interactions mainly through a few side groups that may form some intramolecular H bonds. For completeness, we also report in Fig. 3 the first metastable geometry obtained in the armchair (16, 16) SWNT: again, we find a ring-like conformation if the nanotube is viewed end-on, like in the most stable state found inside this nanotube, but the oligopeptide is slightly more elongated in the direction of the nanotube axis.

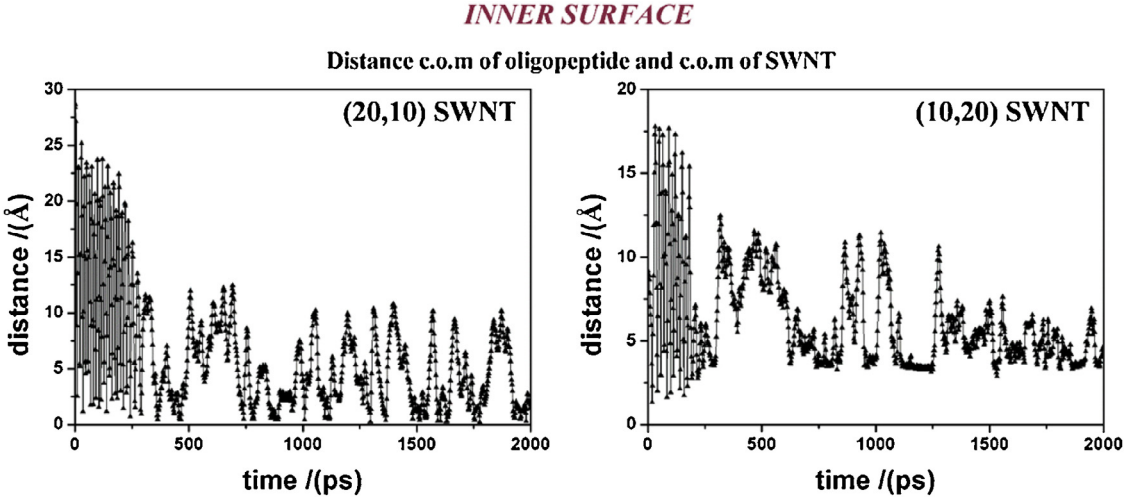

Fig. 4. The distance between the c.o.m. of the oligopeptide and the c.o.m. of the (20, 10) SWNT (at left) and of the (10, 20) SWNT (at right) plotted as a function of time in the MD run that yielded the most stable adducts for either nanotube on the inner surface, as shown in Fig. 3.

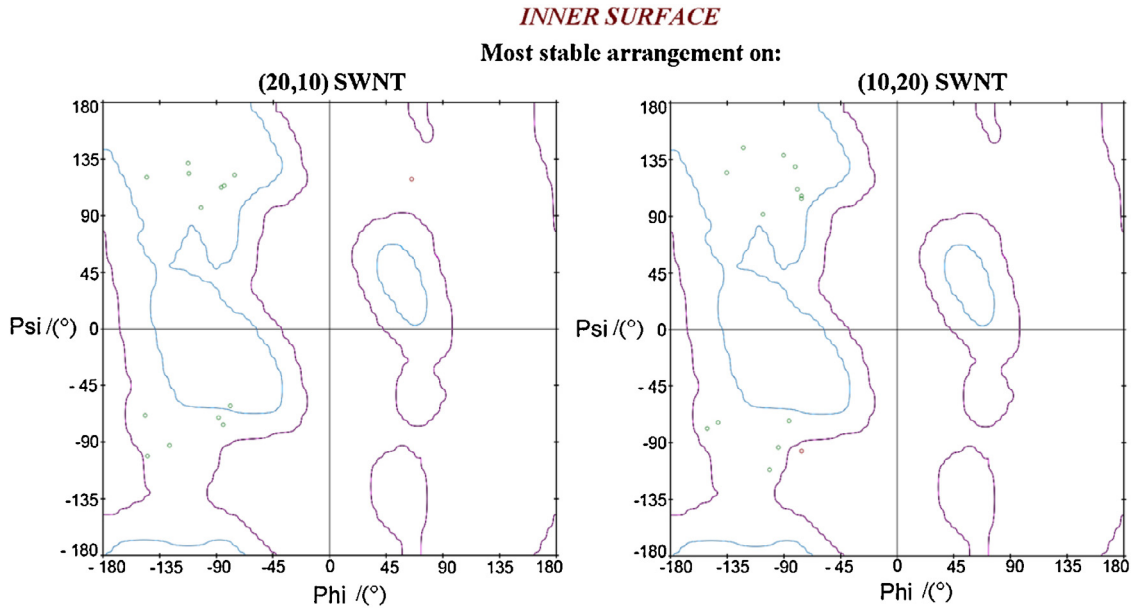

Fig. 5. The Ramachandran maps for the most stable arrangement achieved on the (20, 10) SWNT (at left) and on the enantiomeric (10, 20) SWNT (at right), corresponding to the geometries shown in Fig. 3. The blue and red lines in the Ramachandran plot have the same meaning as in Fig. 1. (For interpretation of the references to color in this figure legend, the reader is referred to the web version of this article.)

Let us conclude this paragraph by pointing out that the unlike stability of the oligopeptide on the concave surface of the enantiomeric SWNT leads to apparently different conformations, as discussed before (see Fig. 3). It must be noted, however, that the different conformations are not due to a different overall distribution of torsion angles (see for instance Figs. S3*b*–S5*b*), but to a different sequence. In fact, the Ramachandran maps obtained for these conformations, reported in Fig. 5. are quite undistinguishable, both showing a strong decrease of the populated region with Ψ being within the -30° to -60° range, and a marked increase in the -90° to -50° range, and in the 90°–150° range quite close to the region typical of a β-sheet secondary structure.

3.3. Interaction on the outer surface of the SWNT

When the oligopeptide was placed in the vicinity of the lateral surface of the nanotube in its native α-helical structure adopting the four different starting orientations described before (Fig. S1*b*), the initial optimizations led in some cases to quite large conformational rearrangements, in particular for the starting geometries where the helical axis was perpendicular to the surface (see Fig. S6). In any case, however, this initial adsorption stage produced relatively weak interactions involving only a few residues, mainly the hydrophobic ones. Therefore, in this case no major changes in the secondary structure are observed after the initial optimization mainly due to the energy penalty implied by disrupting the helical structure.

The molecular dynamics simulations were carried out as before starting with the most and the least stable geometry obtained in the preliminary optimizations, monitoring the equilibration as said before (see for instance Figs. S7*a*–S9*a*). In all cases, the oligopeptide showed a full spreading so as to optimally wrap the nanotubes with all residues being in contact with the surface. As anticipated, we again found a larger stability on the (20, 10) than on the (10, 20) SWNT, while the stability on the (16, 16) is the basically the same as on the former SWNT. In fact, as shown in Table 2, the interaction energy E_{int} on the (20, 10) and on the (16, 16) SWNT is basically the same, the difference between the two values (2 kJ/mol) being hardly significant, since also the difference between the corresponding average potential energies E_{pot} is not significant at the 2σ level, considering the reported standard errors, and even more so if we consider the standard deviations around the mean due to the thermal fluctuations. Furthermore, since in all cases all the 16 residues were found to be in contact with the outer convex surface, also the intrinsic E_{int} follows the same trend, being lower for the interaction on the (20, 10) than on the enantiomeric (10, 20) SWNT; moreover, on the latter SWNT the most stable state is less favorable than both the most stable and the first metastable state on the former SWNT. It should also be noted that the present results on the outer convex surface follow again the previously reported general trend [13]: the surface interaction becomes weaker with an increasing radius of curvature of the surface, and in fact all the present result for E_{int} fall anyway in between those for the (8, 8) and (10, 10) SWNT and those for a single flat sheet of graphite, which has an infinite radius of curvature, thus corresponding to a nanotube with an infinite diameter.

Let us now briefly consider the oligopeptide conformation in the most stable states achieved on the three SWNT, reported in Fig. 6. The most stable arrangement achieved on the (20, 10) SWNT shows a hairpin conformation of the backbone allowing its two halves to interact favorably through the polar side groups that tightly interdigitate to optimize their dipolar interactions. At the same time, the hydrophobic side groups are kept outside the hairpin, strongly interacting with the carbon surface for instance through a parallel arrangement of the aromatic rings. A similar overall conformation is achieved in the most stable state of the (10, 20) SWNT, where adsorption is less favorable than on the enantiomeric nanotube. In this case, however, the hairpin conformation of the backbone most likely induced by the opposite chirality of the nanotube involves the interaction of the hydrophobic side groups with only a protonated LYS residue: only dispersion interactions are thus present, without the extra dipolar stabilization found on the (20, 10) SWNT. Interestingly, on the armchair (16, 16) SWNT the most stable conformation is more elongated than on the chiral nanotube, as it can be easily seen from Fig. 6: in this conformation, the side groups optimize the interaction with the surface and with the topological neighboring residues only, but may form two intramolecular

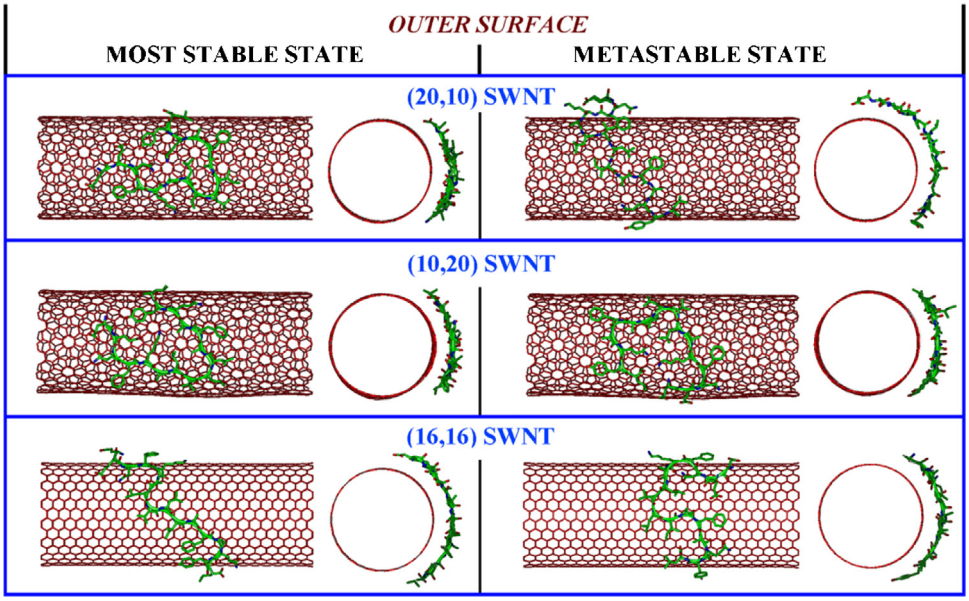

Fig. 6. The most stable (left column) and the metastable state (right column) achieved by the oligopeptide on the outer surface of the (20, 10), the (10, 20) and the (16, 16) SWNT (top to bottom) viewed side on and end on in each case.

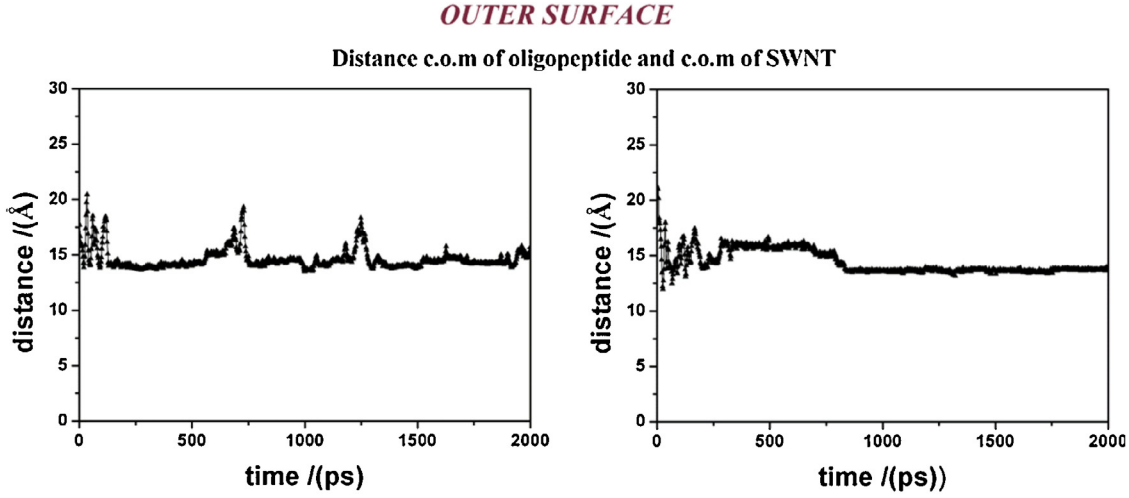

Fig. 7. The distance between the c.o.m. of the oligopeptide and the c.o.m. of the (20, 10) SWNT (at left) and of the (10, 20) SWNT (at right) plotted as a function of time in the MD run that yielded the most stable adducts on the outer surface for either nanotube.

H bonds that contribute to yield a very stable adsorption geometry.

For completeness, in Fig. 6 we also report the oligopeptide conformation in the first metastable state: as it can be seen, no major differences in the backbone conformation are found, and the difference in stability is due to the various combinations of the factors discussed before (dipolar or dispersive interactions only, and possibility of making one or two H bonds). It is, however, noteworthy that on the (20, 10) SWNT the backbone may assume a hairpin conformation (most stable state) or an elongated conformation (first metastable state), but both these arrangements are again more favorable than the most stable one on the (10, 20) SWNT (see Table 2), in keeping with what obtained for the inner surface of the same enantiomeric nanotubes.

It may also be observed that after the initial surface rearrangement the oligopeptide strongly interacts with the surface through all its residues, so that for instance the distance between the c.o.m. of the adsorbate and the c.o.m. of the nanotube are basically the same on either enantiomeric SWNT, and both are featureless at long simulations time, as shown in Fig. 7.

4. Concluding remarks

In this work, we investigate through atomistic molecular dynamics simulations the enantiomeric recognition of two chiral enantiomeric single-walled carbon nanotubes with an opposite handedness by the non-covalent adsorption of a hydrophobic oligopeptide taken from human serum albumin, where in the native state it assumes an α-helical structure. This oligopeptide contains 16 natural amino acids, all having a chiral C_α atom (glycine is not present), so that its adsorption on enantiomeric nanotubes yields different non-covalent complexes that have in principle an unlike stability. We modeled adsorption of this chiral oligopeptide on two enantiomeric single-walled carbon nanotubes, the (20, 10) and the (10, 20) nanotubes, considering also for a comparison the non-chiral (16, 16) armchair nanotube with a very similar diameter.

In either case, such diameter closely matched the end-to-end distance of the original native α-helix. In all cases, we initially placed the oligopeptide close to the lateral surface and to the open end of the nanotubes so as to possibly achieve either adsorption on the outer convex surface or insertion within the nanotube cavity with adsorption on the inner concave surface. In either case, the adsorption turns out to be more favorable on the (20, 10) nanotube than on the enantiomeric (10, 20) nanotube, showing that indeed an adsorbate with many chiral centers allows separating them. Moreover, it also turns out that adsorption on the inner surface of the (20, 10) nanotube is not only more favorable than on the inner surface of its enantiomer, but also more favorable than on the inner surface of the non-chiral armchair (16, 16) nanotube, which shows an intermediate behavior. Considering the outer nanotube surface, we found that adsorption on the (20, 10) is more favorable than on the (10, 20) surface, but basically as favorable as on the non-chiral armchair (16, 16) nanotube. Such results are at variance, as said before, with previous results obtained for *trans* 1,2-substituted cyclopropane and cyclohexane [12]. It is interesting to note that these molecules, which contain two asymmetric carbon atoms, are chiral, but still they possess a rotational symmetry (a C_2 axis), which might explain the predicted lack of enantiomeric discrimination for nanotubes of opposite helicity [12]. We point out that full denaturation and spreading of an oligopeptide with a native α-helix structure inserted in a carbon nanotube is in good agreement with our previous results obtained with larger protein subdomains on the inner and outer surfaces of achiral armchair carbon nanotubes of different diameters [13], where roughly the same conformations were found. Furthermore, we note that the helical interaction with non-chiral armchair nanotubes of different diameters d were recently modeled through molecular dynamics simulations in explicit water, considered a d range of about $15 < d < 35$ Å: for the smaller nanotubes a helical denaturation was observed, even though somewhat less extensive that in our case [24]. More recently, the adsorption of an oligopeptide formed by 12 residues, known to have a strong affinity for carbon nanotubes, onto a flat graphene sheet and on a single (0, 15) nanotube was modeled at the atomistic level [23]. The adsorbed molecule displayed conformational feature quite similar to ours, with the aromatic and the alkyl side groups of hydrophobic residues strongly interacting with the surfaces and the formation of some intramolecular hydrogen bonds involving also the side groups.

We finally stress that the present results are consistent with the separation of enantiomeric nanotubes experimentally achieved in recent years through chiral diporphyrin nano-tweezers [7,8,25] or with a chiral sodium cholate surfactant [9]. Furthermore, our simulations suggest that natural oligopeptides of a sufficiently large size can be used as stationary phases in chromatography for the separation of enantiomeric chiral carbon nanotubes, which may be of huge interest for many technological applications [6]. Furthermore, we point out that a different, and more sophisticated, application of the present results could be envisaged. In fact, the adsorption potentialities of carbon nanotubes [26] and in particular the molecular sieve membranes formed by aligned carbon nanotubes [27,28] have been studied for different applications, including for instance water purification through selective diffusion along the carbon nanotube cavity based on the eluate molecular size and on the nanotube hydrophobicity. The present results suggest that analogous membranes formed by aligned single-walled chiral carbon nanotubes of a given handedness might also act as chromatographic chiral selectors for appropriate racemic mixtures, in particular those involving synthetic oligopeptides containing residues of unlike chiralities. Finally, we note that such membranes may also turn out to be suitable for protein separation as an application in the field of proteomics, because in general a favorable protein–nanotube interaction would yield significantly different retention times.

Acknowledgments

The authors gratefully acknowledge the financial support from MIUR—FIRB Futuro in Ricerca 2008 (RBFR08XH0H).

Appendix A. Supplementary data

Supplementary data associated with this article can be found, in the online version.

References

[1] Tománek, D., The nanotube site: ⟨http://nanotube.msu.edu/⟩.
[2] M.F.L. De Volder, S.H. Tawfick, R.H. Baughman, A.J. Hart, Carbon nano-tubes: present and future commercial applications, Science 339 (2013) 535–539.
[3] N.W. Shi Kam, M. O'Connel, J.A. Wisdom, H. Dai, Carbon nanotubes as multifunctional biological transporters and near-infrared agents for selective cancer cell destruction, Proc. Nat. Acad. Sci. 102 (2005) 11600–11605.
[4] M. Mahmoudi, I. Lynch, M.R. Ejtehadi, M.P. Monopoli, F. Baldelli Bombelli, S. Laurent, Protein–nanoparticle interactions: opportunities and challenges, Chem. Rev. 111 (2011) 5610–5637.
[5] E.B. Barros, A. Jorio, G.G. Samsonidze, R.B. Capaz, A.G. Souza Filho, J. Mendes Filho, G. Dresselhaus, M.S. Dresselhaus, Review on the symmetry-related properties of carbon nanotubes, Phys. Rep. 431 (2006) 261–302.
[6] M.S. Strano, Sorting out left from right, Nat. Nanotechnol. (News Views) 2 (2007) 340–341.
[7] X. Peng, F. Wang, A.K. Bauri, A.F.M.M. Rahman, N. Komatsu, Optical resolution of single-walled carbon nanotubes through molecular recognition with chiral diporphyrin nanotweezers, Chem. Lett. 39 (2010) 1022–1027.
[8] X. Peng, N. Komatsu, S. Bhattacharya, T. Shimawaki, S. Aonuma, T. Kimura, A. Osuka, Optically active single-walled carbon nanotubes, Nat. Nanotechnol. 2 (2007) 361–365.
[9] A.A. Green, M.C. Duch, M.C. Hersam, Isolation of single-walled carbon nanotube enantiomers by density differentiation, Nano Res. 2 (2009) 69–77.
[10] E.M. Pérez, N. Martín, Chiral recognition of carbon nanoforms, Org. Biomol. Chem. 10 (2012) 3577–3583.
[11] G.A. Rance, S.A. Miners, T.W. Chamberlain, A.N. Khlobystov, The effect of carbon nanotubes on chiral chemical reactions, Chem. Phys. Lett. 557 (2013) 10–14.
[12] T.D. Power, A.I. Skoulidas, D.S. Sholl, Can chiral single-walled carbon nanotubes be used as enantiospecific adsorbents? J. Am. Chem. Soc. 124 (2002) 1858–1859.
[13] G. Raffaini, F. Ganazzoli, Surface topography effects in protein adsorption on nanostructured carbon allotropes, Langmuir 29 (2013) 4883–4893.
[14] G. Raffaini, F. Ganazzoli, A simulation study of the interaction of some albumin sub-domains with a flat graphite surface, Langmuir 19 (2003) 3403–3412.
[15] G. Raffaini, F. Ganazzoli, Molecular dynamics simulation of the adsorption of a fibronectin module on a graphite surface, Langmuir 20 (2004) 3371–3378.
[16] G. Raffaini, F. Ganazzoli, Protein adsorption on a hydrophobic surface: a molecular dynamics study of lysozyme on graphite, Langmuir 26 (2010) 5679–5689.
[17] G. Raffaini, F. Ganazzoli, Protein adsorption on the hydrophilic surface of a glassy polymer: a computer simulation study, Phys. Chem. Chem. Phys. 8 (2006) 2765–2772.
[18] G. Raffaini, F. Ganazzoli, L. Malpezzi, C. Fuganti, G. Fronza, W. Panzeri, A. Mele, Validating a strategy for molecular dynamics simulations of cyclodextrin inclusion complexes through single-crystal X-ray and NMR experimental data: a case study, J. Phys. Chem. B 113 (2009) 9110–9122.
[19] T. Wei, M.A. Carignano, I. Szleifer, Lysozyme adsorption on polyethylene surfaces: why are long simulations needed? Langmuir 27 (2011) 12074–12081.
[20] G. Zuo, X. Zhou, Q. Huang, H. Fang, R. Zhou, Adsorption of villin headpiece onto graphene, carbon nanotube, and C60: effect of contacting surface curvatures on binding affinity, J. Phys. Chem. C 115 (2011) 23323–23328.
[21] Accelrys Inc. InsightII 2000. San Diego, CA: Materials Studio and Discovery Studio. See also the URL ⟨http://www.accelrys.com⟩.
[22] P. Dauber-Osguthorpe, V.A. Roberts, D.J. Osguthorpe, J. Wolff, M. Genest, A.T. Hagler, Structure and energetics of ligand binding to proteins: *Escherichia coli* dihydrofolate reductase-trimethoprim, a drug-receptor system, Proteins: Struct. Funct. Genet. 4 (1988) 31–47.
[23] G. Gianese, V. Rosato, F. Cleri, M. Celino, P. Morales, Atomic-scale modeling of the interaction between short polypeptides and carbon surfaces, J. Phys. Chem. B 113 (2009) 12105–12112.
[24] E.J. Sorin, V.S. Pande, Nanotube confinement denatures protein helices, J. Am. Chem. Soc. 128 (2006) 6316–6317.
[25] G. Liu, F. Wang, S. Chaunchaiyakul, Y. Saito, A.K. Bauri, T. Kimura, Y. Kuwahara, N. Komatsu, Simultaneous discrimination of diameter, handedness, and

metallicity of single-walled carbon nanotubes with chiral diporphyrin nanocalipers, J. Am. Chem. Soc. 135 (2013) 4805–4814.
[26] P. Kondrattyuk, J.T. Yates Jr., Molecular views of physical adsorption inside and outside of single-wall carbon nanotubes, Acc. Chem. Res. 40 (2007) 995–1004.
[27] C. Buzea, I.I. Pacheco, K. Robbie, Nanomaterials and nanoparticles: sources and toxicity, Biointerphases 2 (2007) MR17–MR71.
[28] R. Das, M.E. Ali, S.B.A. Hamid, S. Ramakrishna, Z.Z. Chowdhury, Carbon nanotube membranes for water purification: a bright future in water desalination, Desalination 336 (2014) 97–109.
[29] J. Kyte, R.F. Doolittle, A simple method for displaying the hydropathic character of a protein, J. Mol. Biol. 157 (1982) 105–132.